



HAL
open science

Universal Scaling of the Quantum Conductance of an Inversion-Symmetric Interacting Model

Axel Freyn, Jean-Louis Pichard

► **To cite this version:**

Axel Freyn, Jean-Louis Pichard. Universal Scaling of the Quantum Conductance of an Inversion-Symmetric Interacting Model. *Physical Review B: Condensed Matter and Materials Physics* (1998-2015), 2010, 81 (8), pp.085108. 10.1103/PhysRevB.81.085108 . hal-00454373

HAL Id: hal-00454373

<https://hal.science/hal-00454373>

Submitted on 8 Feb 2010

HAL is a multi-disciplinary open access archive for the deposit and dissemination of scientific research documents, whether they are published or not. The documents may come from teaching and research institutions in France or abroad, or from public or private research centers.

L'archive ouverte pluridisciplinaire **HAL**, est destinée au dépôt et à la diffusion de documents scientifiques de niveau recherche, publiés ou non, émanant des établissements d'enseignement et de recherche français ou étrangers, des laboratoires publics ou privés.

Universal Scaling of the Quantum Conductance of an Inversion-Symmetric Interacting Model

Axel Freyn

*Institut Néel, 25 avenue des Martyrs, BP 166, 38042 Grenoble, France and
Service de Physique de l'État Condensé (CNRS URA 2464),
IRAMIS/SPEC, CEA Saclay, 91191 Gif-sur-Yvette, France*

Jean-Louis Pichard

*Service de Physique de l'État Condensé (CNRS URA 2464),
IRAMIS/SPEC, CEA Saclay, 91191 Gif-sur-Yvette, France*

We consider quantum transport of spinless fermions in a 1D lattice embedding an interacting region (two sites with inter-site repulsion U and inter-site hopping t_d , coupled to leads by hopping terms t_c). Using the numerical renormalization group for the particle-hole symmetric case, we study the quantum conductance g as a function of the inter-site hopping t_d . The interacting region, which is perfectly reflecting when $t_d \rightarrow 0$ or $t_d \rightarrow \infty$, becomes perfectly transmitting if t_d takes an intermediate value $\tau(U, t_c)$ which defines the characteristic energy of this interacting model. When $t_d < t_c\sqrt{U}$, g is given by a universal function of the dimensionless ratio $X = t_d/\tau$. This universality characterizes the non-interacting regime where $\tau = t_c^2$, the perturbative regime ($U < t_c^2$) where τ can be obtained using Hartree-Fock theory, and the non-perturbative regime ($U > t_c^2$) where τ is twice the characteristic temperature T_K of an orbital Kondo effect induced by the inversion symmetry. When $t_d < \tau$, the expression $g(X) = 4(X + X^{-1})^{-2}$ valid without interaction describes also the conductance in the presence of the interaction. To obtain those results, we map this spinless model onto an Anderson model with spins, where the quantum impurity is at the end point of a semi-infinite 1D lead and where t_d plays the role of a magnetic field h . This allows us to describe $g(t_d)$ using exact results obtained for the magnetization $m(h)$ of the Anderson model at zero temperature. We expect this universal scaling to be valid also in models with 2D leads, and observable using 2D semi-conductor heterostructures and an interacting region made of two identical quantum dots with strong capacitive inter-dot coupling and connected via a tunable quantum point contact.

PACS numbers: 71.10.-w, 72.10.-d, 73.23.-b

Introduction

In quantum transport theory, a nanosystem inside which the electrons do not interact has a zero temperature conductance which is given (in units of the conductance quantum e^2/h for spin polarized electrons, $2e^2/h$ with spin degeneracy) by

$$g = |t_{ns}(E_F)|^2, \quad (1)$$

where $|t_{ns}(E_F)|^2$ is the probability for an electron at the Fermi energy E_F to be transmitted through the nanosystem. This Landauer-Büttiker formula can be extended^{1,2} to an interacting nanosystem, if it behaves as a non-interacting nanosystem with renormalized parameters as the temperature $T \rightarrow 0$. However, this effective non-interacting nanosystem does not describe only the interacting region, but depends also on the presence of scatterers which can be outside, in the attached leads. This non-local aspect of the effective transmission $|t_{ns}(E_F)|^2$ is characteristic of nanosystems inside which electrons interact and has been studied in 1D models^{3,4} using the density matrix renormalization group (DMRG), and in 1D⁵⁻⁷ and 2D models⁸ using the Hartree-Fock (HF) approximation.

In this work, we study how the effective transmission of a nanosystem with perfect leads is renormalized by local interactions acting inside the nanosystem, using the numerical renormalization group (NRG) algorithm⁹⁻¹³ and an inversion-symmetric interacting model (ISIM). This model describes the scattering of spin-polarized electrons (spinless fermions) by an interacting region (two sites characterized by an inter-site

hopping term t_d , coupling terms t_c and an inter-site repulsion U). Our study is restricted to the symmetric case (i.e. the case where ISIM is invariant under particle-hole symmetry).

Firstly, we prove that ISIM, which is perfectly reflecting when the inter-site hopping term $t_d \rightarrow 0$ or $t_d \rightarrow \infty$, exhibits a peak of perfect transmission for an intermediate value $\tau(U, t_c)$ of t_d . This scale $\tau(U, t_c)$ defines very precisely the fundamental energy scale of ISIM. HF theory gives correctly this peak of perfect transmission when $U < t_c^2$, but does not give it when U exceeds t_c^2 , showing the existence of a non-perturbative regime where the use of the NRG algorithm is required. In this non-perturbative regime,

$$\tau(U, t_c) = 2T_K, \quad (2)$$

where T_K is the characteristic temperature of an orbital Kondo effect induced by the inversion symmetry.

Secondly, we show that the zero-temperature conductance g is given by a universal function $g(X)$ of the dimensionless coordinate $X = t_d/\tau$. This function $g(X)$ is independent of the choice of t_c and U as far as $t_d < t_c\sqrt{U}$. When $t_d < \tau$,

$$g(X) = 4(X + X^{-1})^{-2}. \quad (3)$$

When $\tau < t_d < t_c\sqrt{U}$, the conductance $g(X)$ can be described by another function

$$g(X) \approx \sin^2 \left(\pi \left(2.02 - \frac{0.74}{\ln(2.8X)} + \dots \right) \right), \quad (4)$$

which is related to an exact result obtained by Tsvetlick and Wiegmann^{14,15} with Bethe-Ansatz for the magnetization of the Anderson model at zero temperature. When t_d exceeds $t_c\sqrt{U}$, the interaction becomes irrelevant, τ is given by its non-interacting value t_c^2 , $X = t_d/t_c^2$ and $g(X) = 4(X + X^{-1})^{-2}$ again. The conductance g is one example of the physical properties of ISIM which are given by universal functions of t_d/τ at zero temperature. The low-energy effective one-body excitations provide another example for which we show the corresponding universal curves.

In order to obtain these universal functions, it is useful to notice that the inversion symmetry of ISIM gives rise to a pseudo-spin, allowing to exactly map this 1D spinless model onto an Anderson model with spins where the inter-site hopping t_d plays the role of a magnetic field, the quantum impurity being at the end point of a single semi-infinite chain. Therefore, the behavior of ISIM as a function of t_d is related to the behavior of the Anderson model as a function of an applied magnetic field h .

The paper is organized as follows: Section I introduces universal aspects which characterize the Anderson model and are relevant for quantum dots where spin or orbital Kondo effects occur. The studied spinless model with inversion symmetry (ISIM) is defined in section II and mapped onto an Anderson model with magnetic field in section III. A second transformation is performed in section IV, based on the usual logarithmic discretization of the energy band of the leads, to get the final model used for the NRG study. The study is restricted to the case with particle-hole symmetry in section V. The low energy excitations are first considered as a function of the temperature in section VI. When $U > \pi\Gamma$, $\Gamma = t_c^2$ being the level width of the scattering region, the 3 fixed points [free orbital (FO), local moment (LM) and strong coupling (SC)] characterizing the Anderson model without field are recovered when t_d is small enough. As t_d increases, the LM fixed point characterizing the model above the Kondo temperature T_K disappears. In section VII, we study the low energy excitations of ISIM as a function of t_d in the limit $T \rightarrow 0$. We find that they can always be described by a set of effective one-body excitations, showing that a continuous line of free fermion fixed points goes from the SC limit of the Anderson model ($t_d = 0$) towards a new simple limit: the polarized orbital (PO) fixed point ($t_d \rightarrow \infty$). Between the SC and PO fixed points, we show in section VIII that there is always an intermediate value $\tau(U, t_c)$ of t_d for which ISIM is perfectly transmitting. $\tau(U, t_c)$ defines the fundamental energy scale of ISIM. In section IX, a simple method for calculating $g(t_d)$ from the effective one body excitations characterizing ISIM when $T \rightarrow 0$ is introduced. Using this method, we give in section IX the main result of this work, i.e., if one uses the dimensionless ratio $X = t_d/\tau$, the physical properties (conductance or effective one-body spectra) are universal and independent of t_c and U as far as $t_d < t_c\sqrt{U}$. This universal regime is divided in a first regime where the system is not very far from the SC fixed point ($t_d \leq \tau$, subsection X A) and where $g(X) = 4(X + X^{-1})^{-2}$, followed by a second regime where $g(X)$ is given by another universal function ($\tau \leq t_d < t_c\sqrt{U}$, subsection X B). In the equivalent Anderson model, this second regime is characterized by the

occurrence of a magnetic moment. When $t_d > t_c\sqrt{U}$, the interaction U becomes irrelevant and $g(X) = 4(X + X^{-1})^{-2}$ with $X = t_d/t_c^2$ (subsection X C). In section XI, we show that HF theory gives the values of g obtained from the NRG spectra and the scale $\tau(U, t_c)$, if U does not exceed t_c^2 . In contrast, HF theory fails to give perfect transmission if $U > t_c^2$, showing the existence of a non-perturbative regime for ISIM. To obtain τ in the non-perturbative regime, we first revisit in section XII a method giving g from the difference of occupation numbers between the even and odd orbitals of the nanosystem. This method based on Friedel sum rule (FSR) contains an assumption. If ISIM is near the SC fixed point ($t_d < \tau$, non-perturbative regime), this assumption turns out to be justified. In that case, $g(t_d)$ can be obtained from the impurity magnetization $m(h)$ of the equivalent Anderson model with a magnetic field h at zero temperature. Exact results giving $m(h)$ are reviewed in section XIII for the Anderson model. Using those results, we show in section XIV that $\tau(U, t_c) = 2T_K$ in the non-perturbative regime, T_K being the characteristic temperature of the orbital Kondo effect exhibited by ISIM when $U > t_c^2$. Moreover, a fit inspired from the exact behavior of $m(h)$ in the local moment regime is used for describing the universal function $g(X)$ when $\tau \leq t_d < t_c\sqrt{U}$. Eventually, we summarize in section XV the universal aspects obtained using a simple 1D model, and we conjecture that they can be extended to 2D models and observed in 2D semi-conductor heterostructures, where the nanosystem would consist of two identical quantum dots coupled by a quantum point contact.

I. ANDERSON MODEL, KONDO PHYSICS, QUANTUM DOTS AND UNIVERSALITY

The Anderson model describes a single site with Hubbard interaction U coupled to a 3D bath of conduction electrons. This is one of the quantum impurity models¹³ which were introduced to study the resistance minimum observed in metals with magnetic impurities. The Kondo problem refers to the failure of perturbative techniques to describe this minimum. The solution of these models by the NRG algorithm, a non-perturbative technique⁹⁻¹³ introduced by Wilson, is at the origin of the discovery of universal behaviors which can emerge from many-body effects. Without magnetic field h and with particle-hole symmetry¹⁰, the Anderson model maps onto the Kondo Hamiltonian if $U > \pi\Gamma$, $\Gamma \propto t_c^2$ being the impurity-level width. In that case, there is a non-perturbative regime where the temperature dependence of physical observables such as the impurity susceptibility is given by universal functions of T/T_K , T_K being the Kondo temperature. If $U < \pi\Gamma$, the impurity susceptibility can be obtained by perturbation theory. Universality characterizes not only the behavior of the Anderson model as a function of the temperature T , but also its behavior at $T = 0$ as a function of an applied magnetic field h . Using the Bethe-Ansatz, Tsvetlick and Wiegmann^{14,15} have obtained for the magnetization $m(h)$ a universal function of the dimensionless variable h/T_K when $T \rightarrow 0$.

The possibility to design artificial magnetic impurities in

nanoscale conductors has opened^{16,17} a second era for quantum impurity models. Measuring the conductance g of quantum dots created by electrostatic gates, in a 2D electron gas^{16–18} or in carbon nanotubes¹⁹, one obtains values which can be on universal curves as functions of T/T_K if there is a Kondo effect. Moreover, quantum dots open the possibility to study the Kondo effect as a function of the coupling between the impurity and the continuum of conduction electrons, and not only as functions of the temperature and of the magnetic field. As pointed out in Ref. 20, this gives the opportunity to do the spectroscopy of the Kondo problem. Notably, the weak to strong coupling crossover can be studied by varying gate voltages, when metallic gates are used for creating quantum dots. Kondo physics was first related to the anti-ferromagnetic coupling between a magnetic impurity and the spin of the host's conduction electrons. This is why Kondo physics was first expected and seen^{16,17} in quantum dots with odd numbers of electrons, weakly coupled to leads. However, it was realized that a localized electronic state coupled to a continuum can give rise to a large class of different Kondo effects, including the original spin-1/2 Kondo effect, various orbital Kondo effects and the SU(4) Kondo effect occurring if a spin Kondo effect co-exists with an orbital Kondo effect.

In this framework, ISIM is a model which can be used for describing the quantum conductance of spin polarized electrons in an inversion-symmetric double-dot setup with strong capacitive inter-dot coupling, as a function of the inter-dot hopping t_d . For such a setup, t_d could be varied by electrostatic gates if the two dots are coupled by a quantum point contact, and our study describes the effect of this coupling upon the orbital Kondo effect induced by the inversion symmetry. Eventually, universal aspects of many-body phenomena characterize not only equilibrium quantum transport, but also non-equilibrium quantum transport which occurs in the presence of a large source-drain bias V_{sd} . Measures of the conductance¹⁸ and of the current noise¹⁹ of Kondo dots have recently confirmed the expected universality if one measures T or V_{sd} in units of T_K . We describe here another universal aspect of linear quantum transport, i.e., the quantum conductance of a spin polarized inversion symmetric double-dot setup should be a universal function of the dimensionless inter-dot hopping t_d/T_K when $T \rightarrow 0$.

Kondo physics is also at the origin of spinless models, as the interacting resonant level model²¹ (IRLM) which describes a resonant level ($V_d d^\dagger d$) coupled to two baths of spinless electrons via tunneling junctions and an interaction U between the level and the baths. IRLM, which is now used for studying non-equilibrium quantum transport^{21,22}, is related to the Kondo model, the charge states $n_d = 0, 1$ playing the role of spin states. Both ISIM and IRLM are inversion symmetric. However, the Zeeman field acting on the impurity is played by the hopping term t_d for ISIM, and by the site energy V_d for IRLM. Therefore, ISIM does not transmit the electrons without “field”, while IRLM does. Though we study in this work a finite density of particles, let us mention that the two-particle scattering problem has been solved²³ for ISIM.

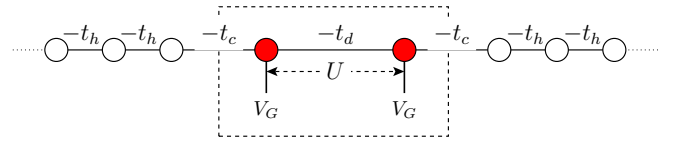


FIG. 1: (Color online) Studied setup (ISIM) where spin polarized electrons (spinless fermions) can be scattered by a nanosystem made of the 2 red sites (energy V_G , inter-site repulsion U and an internal hopping t_d). The nanosystem is embedded by coupling terms t_c into a 1D lattice (hopping term t_h).

II. INVERSION-SYMMETRIC INTERACTING MODEL

The ISIM model is sketched in Fig. 1 and consists of a 1D tight binding lattice (hopping term t_h) where a finite density of spin polarized electrons (spinless fermions) can be scattered by a central region made of 2 sites of potential V_G , with an internal hopping term t_d , and 2 coupling terms t_c . The difficulty comes from the presence of a repulsion of strength U which acts if the two sites of the central region are occupied.

The ISIM Hamiltonian reads:

$$H = H_{ns} + H_c + H_l, \quad (5)$$

where the Hamiltonian of the central region (the interacting nanosystem) is given by

$$H_{ns} = -t_d (c_0^\dagger c_1 + c_1^\dagger c_0) + V_G (n_0 + n_1) + U n_0 n_1. \quad (6)$$

c_x^\dagger and c_x are spinless fermion operators at site x and $n_x = c_x^\dagger c_x$. The coupling Hamiltonian between the nanosystem and the leads reads

$$H_c = -t_c (c_{-1}^\dagger c_0 + c_1^\dagger c_2 + H.c.), \quad (7)$$

while the leads are described by an Hamiltonian

$$H_l = -t_h \sum_{x=-\infty}^{\infty} (c_x^\dagger c_{x+1} + H.c.), \quad (8)$$

where \sum' means that $x = -1, 0, 1$ are omitted from the summation.

III. EQUIVALENT ANDERSON MODEL WITH MAGNETIC FIELD

Because of inversion symmetry, one can map ISIM onto a single semi-infinite 1D lattice where the fermions have a pseudo-spin and where the double-site nanosystem becomes a single site with Hubbard repulsion U at the end point of a semi-infinite lattice. This equivalent Anderson model is sketched in Fig. 2. To show this mapping, we define the fermion operators

$$a_{e,x}^\dagger = (c_{-x+1}^\dagger + c_x^\dagger)/\sqrt{2}, \quad (9)$$

$$a_{o,x}^\dagger = (c_{-x+1}^\dagger - c_x^\dagger)/\sqrt{2}, \quad (10)$$

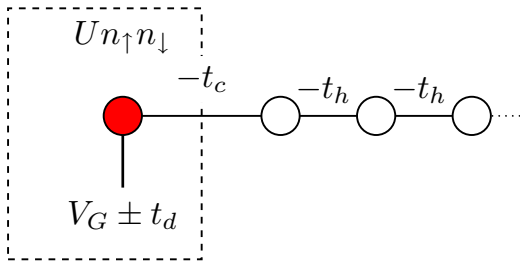


FIG. 2: (Color online) Equivalent Anderson model: Electrons with a pseudo spin ($\uparrow = \text{even}$, $\downarrow = \text{odd}$) are free to move on a semi-infinite chain (hopping term t_h) with a quantum impurity (red site) attached (hopping term t_c) to its end point. The inter-site ISIM interaction becomes a Hubbard interaction $U n_{\uparrow} n_{\downarrow}$ between impurity orbitals of different pseudo-spins. The impurity potential V_G has now a Zeeman term $\pm t_d$.

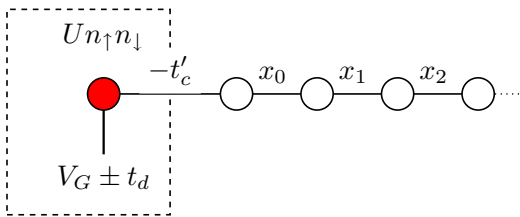


FIG. 3: (Color online) Corresponding NRG chain: The quantum impurity (red site) is now coupled via an hopping term t'_c (Eq. (19)) to a 1D lattice, where the sites are labelled by n and describe conduction electron excitations of length scale $\Lambda^{n/2} k_F^{-1}$ centered on the impurity. The successive sites are now coupled via hopping terms (Eq. (18)) which fall off as $\Lambda^{-n/2}$. Used discretization parameter $\Lambda = 2$.

which create a spinless fermion in an even/odd (e/o) combination of the orbitals located at the sites x and $-x+1$ of the original infinite lattice, (or a fermion with pseudo-spin $\sigma = e/o$ in the transformed semi-infinite lattice). $a_{e/o,x}$ are the corresponding annihilation operators. Expressing H_{ns} in terms of these new operators, one gets

$$H_{ns} = (V_G - t_d)n_e + (V_G + t_d)n_o + U n_e n_o, \quad (11)$$

where $n_{\sigma} = a_{\sigma,1}^{\dagger} a_{\sigma,1}$ and where the pseudo-spin “e” (“o”) is parallel (anti-parallel) to the “Zeeman field” t_d . In terms of the operators

$$d_{k,\sigma}^{\dagger} = \sqrt{2/\pi} \sum_{x=2}^{\infty} \sin(k(x-1)) a_{\sigma,x}^{\dagger} \quad (12)$$

creating a spinless fermion of pseudo-spin σ and momentum k in the transformed semi-infinite 1D-lead, the lead and the coupling Hamiltonians can be written as

$$H_l = \sum_{k,\sigma} \epsilon_k n_{k,\sigma} \quad (13)$$

and

$$H_c = \sum_{k,\sigma} V(k) (a_{\sigma,1}^{\dagger} d_{k,\sigma} + H.c.), \quad (14)$$

where the k -dependent hybridization

$$V(k) = -t_c \sqrt{2/\pi} \sin k \quad (15)$$

yields an impurity level width at E_F which is given by

$$\Gamma = \frac{t_c^2}{t_h} \sin k_F, \quad (16)$$

$n_{k,\sigma} = d_{k,\sigma}^{\dagger} d_{k,\sigma}$ and $\epsilon_k = -2t_h \cos k$.

One can see that ISIM is identical to an Anderson model with a local magnetic field t_d which acts on the impurity only and gives rise to the Zeeman terms $\pm t_d$ in Eq. (11). Therefore, in the limit $t_d \rightarrow 0$, ISIM must exhibit an orbital Kondo effect if the equivalent Anderson model can be reduced to a Kondo model. The fact that the impurity is not coupled to a 3D bath of conduction electrons, but only to a single semi-infinite 1D bath changes only the proportionality factor of the hybridization function. We underline that the dimensionality of the considered baths of conduction electrons does not play a significant role in Kondo physics, such that the results of this study should hold if one attaches 2D bars or 3D strips instead of 1D leads to the same nanosystem.

IV. CORRESPONDING NRG CHAIN

ISIM can be studied using the NRG procedure^{10,12,13} developed by Wilson for the Anderson model after minor changes. First, we assume $V(k) \approx V(k_F = \pi/2)$ and, using standard NRG procedure, we divide the conduction band of the electron bath into logarithmic sub-bands characterized by an index n and an energy width

$$d_n = \Lambda^{-n} (1 - \Lambda^{-1}). \quad (17)$$

Throughout this paper, we use the discretization parameter $\Lambda = 2$. Within each sub-band, we introduce a complete set of orthonormal functions $\psi_{np}(\epsilon)$, and expand the lead operators in this basis. Dropping the terms with $p \neq 0$ and using a Gram-Schmidt procedure, the original 1D leads give rise to another semi-infinite chain with nearest-neighbor hopping terms, each site n representing now a conduction electron excitation at a length scale $\Lambda^{n/2} k_F^{-1}$ centered at the impurity. In this transformed 1D model shown in Fig. 3 and hereafter called the NRG chain, the impurity and the $N-1$ first sites form a finite chain of length N , which is described by the Hamiltonian H_N , the successive sites n and $n+1$ being coupled by hopping terms x_n which decay exponentially as $n \rightarrow \infty$ and are given by:

$$x_n = \Lambda^{-n/2} \frac{(1 + \Lambda^{-1})(1 - \Lambda^{-n-1})}{2\sqrt{(1 - \Lambda^{-2N-1})(1 - \Lambda^{-2N-3})}}. \quad (18)$$

The impurity is coupled to the first site of the NRG chain by an hopping term

$$t'_c = \frac{t_c}{(8\pi^3)^{1/4}} \left(\log \left(\frac{\Lambda(\Lambda+1)}{\Lambda-1} \right) \right)^2. \quad (19)$$

Since the length N is related¹⁰ to the temperature T by the relation

$$k_B T \approx \frac{1 + \Lambda^{-1}}{2} \Lambda^{-(N-1)/2}, \quad (20)$$

N can be interpreted as a logarithmic temperature scale ($N \propto -\log T$), the large values of N corresponding to temperatures T small compared to the bandwidth t_h .

The NRG chain coupled to the impurity is iteratively diagonalized and rescaled, the spectrum being truncated to the N_s first states at each iteration (We use $N_s = 1024$ in this study). The behavior of ISIM as T decreases can be obtained from the spectrum of H_N as N increases, the bandwidth of H_N being suitably rescaled at each step. A fixed point of the renormalization group (RG) flow corresponds to an interval of successive iterations N of the same parity, where the rescaled many-body excitations $E_I(N)$ do not vary. The fixed point is therefore characterized inside this interval by two spectra, one characterizing the even values of N , the other the odd values. If it is a free fermion fixed point, $E_I = \sum_{\alpha} \epsilon_{\alpha}$, the ϵ_{α} being effective one-body excitations, and the interacting system behaves as a non-interacting system with renormalized parameters \tilde{t}_d and \tilde{t}_c near the fixed point. Moreover, if one has free fermions when $T \rightarrow 0$, the conductance g can be directly extracted from the NRG spectrum.

V. RESTRICTION TO THE SYMMETRIC CASE

Using the NRG procedure, ISIM can be studied as a function of T for arbitrary values of its 6 bare parameters U , E_F , V_G , t_d , t_c and t_h . Hereafter, we take $E_F = 0$ and $V_G = -U/2$. This choice makes ISIM invariant under particle-hole symmetry, with a uniform density $\langle n_x \rangle = 1/2$. Very often, the infinite bandwidth limit ($t_h \rightarrow \infty$) is assumed in the theory of quantum impurities. This corresponds to magnetic alloys where the bandwidth of the conduction electrons is large compared to the other energy scales of the model. In this study, we take $t_h = 1$, which defines the energy scale and allows us to consider also mesoscopic regimes where the scales U , t_d , t_c or V_G can exceed t_h . In that case, Eq. (16) gives for the levels $\pm t_d$ of the isolated non-interacting nanosystem a width

$$\Gamma = t_c^2 \quad (21)$$

when the nanosystem is coupled to leads. Our motivation to restrict the study to the symmetric case is not justified by physical considerations, but mainly for the sake of simplicity, restricting the RG flow into a space of 3 effective parameters (\tilde{U} , \tilde{t}_c , \tilde{t}_d) only. Doing so, we proceed as Krishna-murthy, Wilkins and Wilson for the Anderson model, studying first the symmetric case¹⁰ before considering later the asymmetric case¹¹ and its characteristic valence-fluctuation regime.

VI. ROLE OF THE TEMPERATURE T

When $t_d = 0$, ISIM is an Anderson model which has the RG flow sketched in Fig. 4 for the particle-hole symmetric

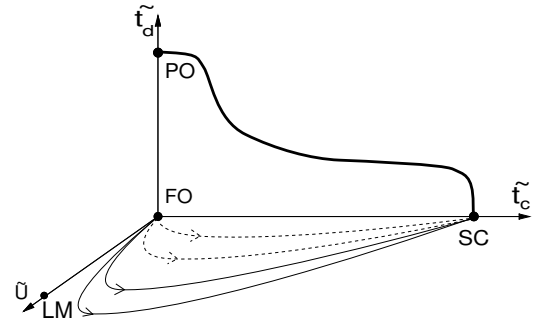


FIG. 4: Line of free fermion fixed points [thick solid line in the plane (\tilde{t}_d, \tilde{t}_c)], characterizing ISIM when $T \rightarrow 0$ as t_d increases from $t_d = 0$ (SC fixed point) towards $t_d \rightarrow \infty$ (PO fixed point). The FO, LM and SC free fermion fixed points and the RG trajectories¹³ followed by ISIM as T decreases for $t_d = 0$ are indicated in the plane (\tilde{U}, \tilde{t}_c), for $\pi\Gamma > U$ (dashed) and $\pi\Gamma < U$ (solid).

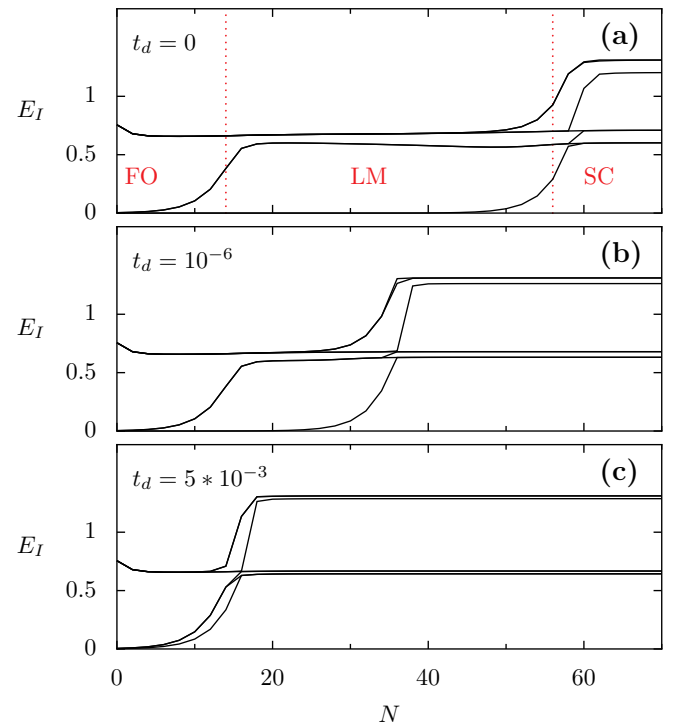


FIG. 5: (Color online) Many body excitations E_I as a function of N (even values) for $U = 0.005$ and $t_c = 0.01$. For $t_d = 0$ (Fig. 5a), one can see the 3 successive plateaus (FO, LM and SC fixed points) of the Anderson model. As t_d increases (Fig. 5b and Fig. 5c), the LM plateau shrinks and disappears when $t_d \gg t_d^* = t_c \sqrt{U}$.

case. At low values of N (high values of T), ISIM is located in the vicinity of the unstable free-orbital (FO) fixed point. As N increases (T decreases), ISIM flows towards the stable strong-coupling (SC) fixed point.

If the interaction is weak ($U < \pi\Gamma$), its effects can be described by perturbation theory, the flow goes directly from the FO fixed point towards the SC fixed point, and there appears no orbital Kondo effect for $t_d \rightarrow 0$.

If the interaction is large ($U > \pi\Gamma$), the flow can visit

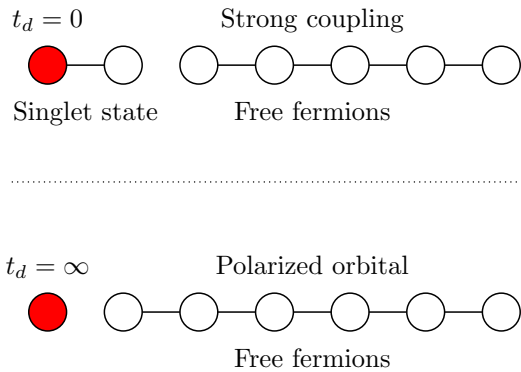


FIG. 6: (Color online) NRG chain in the SC limit (upper figure) and in the PO limit (lower figure). When $t_d \rightarrow 0$, the impurity (red dot) and the first site of the NRG chain form a system in its singlet ground state decoupled from the other sites which carry free fermion excitations. When $t_d \rightarrow \infty$, the even (odd) orbital of the impurity is occupied (empty) and the other sites carry free fermion excitations. Therefore, there is a permutation of the parity of the length of the free part as t_d increases. When the excitations of the free part are independent of this parity, $t_d = \tau$ and $g = 1$.

an intermediate unstable fixed point—the local-moment (LM) fixed point—before reaching the SC fixed point. In that case, ISIM is identical to a Kondo model characterized by a temperature T_K and by universal functions of the ratio T/T_K . For $t_d = 0$, ISIM is on the FO fixed point when $t_c\sqrt{U} < T$, exhibits a local moment when $T_K < T < t_c\sqrt{U}$ and reaches the SC fixed point when $T < T_K$. While the Hartree-Fock theory qualitatively describes²⁴ the local moment at high temperatures $T_K < T < t_c\sqrt{U}$, it breaks down at low temperatures ($T < T_K$), where the effect of the interaction becomes non-perturbative and gives an orbital Kondo effect.

In Fig. 5, the first many-body excitations E_I of ISIM are given for increasing even values of N for $t_d = 0$. Since $U > \pi t_c^2$, one gets 3 plateaus corresponding to the 3 expected fixed points. Inside the plateaus, the spectra are free fermion spectra which are described in Ref. 10. However, between the plateaus, there are no free fermion spectra and $E_I \neq \sum_{\alpha} \epsilon_{\alpha}$. As t_d increases (Fig. 5), the LM plateau decreases and vanishes when t_d reaches a value $\approx t_c\sqrt{U}$.

VII. ROLE OF THE INTERNAL HOPPING AT $T = 0$

Let us study how the many-body levels E_I given by the NRG algorithm depend on the internal hopping term t_d in the limit where $N \rightarrow \infty$, i.e. in the limit where the temperature $T \rightarrow 0$.

When $t_d = 0$, one has the SC limit¹⁰ of the Anderson model where the impurity is strongly coupled to its first neighbor in the NRG chain (the conduction-electron state at the impurity site). The impurity and this site form a system which can be reduced to its ground state (a singlet), the $N - 2$ other sites carrying free fermion excitations ϵ_{α} which are independent of that interacting system. This SC limit of the Anderson model without field is sketched in Fig. 6 (upper part). In the Kondo

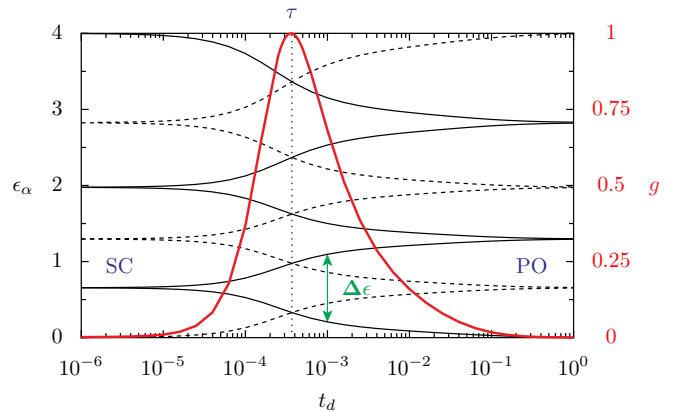


FIG. 7: (Color online) One body excitations $\epsilon_{\alpha}(t_d)$ [extracted from the $E_I(N \rightarrow \infty, t_d)$] for $U = 0.1$ and $t_c = 0.1$ (left scale). The solid (dashed) lines correspond to NRG chains of even (odd) length N . Conductance $g(t_d)$ extracted from $\Delta\epsilon(t_d)$ using Eq. (27) (thick red curve, right scale). For $t_d = \tau$, the ϵ_{α} are independent of the parity of N and $g = 1$.

model, the site directly coupled to the impurity describes the cloud of conduction electrons which fully screens the magnetic moment of the impurity.

When $t_d \rightarrow \infty$, the impurity occupation numbers $\langle n_e \rangle \rightarrow 1$ and $\langle n_o \rangle \rightarrow 0$, and the $N - 1$ other sites of the NRG chain are independent of the impurity. This limit is sketched in Fig. 6 (lower part). We call this limit “Polarized Orbital (PO),” since it coincides with the FO fixed point of the Anderson model, except that the spin of the free orbital is not free, but fully polarized in our case.

The $E_I(t_d)$ correspond to many-body excitations of effective non-interacting spectra when $t_d \rightarrow 0$ and $t_d \rightarrow \infty$. When t_d varies between those 2 limits, the NRG algorithm continues to give many-body excitations $E_I(t_d)$ compatible with the free fermion rule $E_I(t_d) = \sum_{\alpha} \epsilon_{\alpha}(t_d)$, allowing us to extract one-body excitations $\epsilon_{\alpha}(t_d)$ for intermediate values of t_d . We conclude that there is a continuum of effective non-interacting spectra which describe the E_I as t_d varies in the limit $N \rightarrow \infty$, i.e. the $T \rightarrow 0$ limit of ISIM is given by a continuum line of free fermion fixed points. This line is sketched in Fig. 4. Having always free fermions as t_d varies means that the $T = 0$ scattering properties of an interacting region embedded inside an infinite non-interacting lattice are those of an effective non-interacting system with renormalized parameters, in agreement with the DMRG study of the persistent current given in Ref. 2. We underline that those effective non-interacting spectra describe the $T = 0$ limit, while a description of the low-temperature dependence of the conductance requires effective Hamiltonians of Landau quasiparticles with residual quasiparticle interactions. Such a Fermi liquid theory has been proposed by Nozières. In the case of the Anderson model, it has been developed in Ref. 25 without magnetic field ($t_d = 0$) and in Ref. 26 with magnetic field ($t_d \neq 0$). However, the quasiparticle interaction comes into play at finite temperatures only and a residual interaction is not necessary for describing the E_I as a function of t_d in the

limit $N \rightarrow \infty$.

Fig. 7 shows these first one-body excitations ϵ_α as a function of t_d extracted from the $E_I(t_d)$, calculated with $U = 0.1$ and $t_c = 0.1$. The pseudo-spin degeneracy being broken by the “magnetic field” $t_d \neq 0$, the first (second) one-body excitation ϵ_1 (ϵ_2) carries respectively an even (odd) pseudo-spin if N is even. This is the inverse if N is odd, ϵ_1 (ϵ_2) carrying respectively an odd (even) pseudo-spin.

VIII. PERFECT TRANSMISSION AND CHARACTERISTIC ENERGY SCALE

Since the free part of the NRG chain has $N - 2$ sites for $N \rightarrow \infty$ and $t_d \rightarrow 0$ (SC fixed point), while it has $N - 1$ sites for $t_d \rightarrow \infty$ (PO fixed point), there is a permutation of the $\epsilon_\alpha(t_d)$ as t_d increases: the $\epsilon_\alpha(t_d \rightarrow 0)$ for N even become the $\epsilon_\alpha(t_d \rightarrow \infty)$ for N odd and vice-versa. This permutation is shown in Fig. 7. Since for $N \rightarrow \infty$ there is a permutation between the even and odd spectra as t_d increases, there is a value of t_d for which the $\epsilon_\alpha(t_d)$ are independent of the parity of N . This value defines very precisely the characteristic energy scale $\tau(U, t_c)$ of ISIM. Because of particle-hole symmetry, the nanosystem (the impurity of the NRG chain) is always occupied by one electron. Binding one electron of the leads with this electron reduces the energy when $t_d < \tau$, while it increases the energy when $t_d > \tau$. For $t_d = \tau$, it is indifferent to bind or not an electron of the lead with the one of the nanosystem, making ISIM perfectly transparent. This gives the proof that, for all values of U and t_c , there is always a value τ of t_d for which the interacting region becomes perfectly transmitting and

$$g(t_d = \tau(U, t_c)) = 1. \quad (22)$$

The argument is reminiscent to that giving the condition for having a perfectly transparent quantum dot in the Coulomb blockade regime: t_d in our case, the gate voltage in the other case, have to be adjusted to values for which it costs the same energy to put an extra electron outside or inside the dot. The quantum conductance g can be extracted from the NRG spectra. Using a method explained in the following section, we have calculated $g(t_d)$. The result shown in Fig. 7 confirms that $g = 1$ precisely for the value τ of t_d for which the $N \rightarrow \infty$ low energy excitations are independent of the parity of N .

IX. FREE-FERMION SPECTRA AND QUANTUM CONDUCTANCE

As pointed out in previous works^{27–29}, the quantum conductance g can be directly extracted from the NRG spectra. Let us consider an NRG chain of even length $N \rightarrow \infty$. When $t_d = 0$, the one body spectrum is identical for the two pseudo-spins. A hopping $t_d \neq 0$ breaks the pseudo-spin degeneracy and opens a gap $\Delta\epsilon(t_d)$ (indicated in Fig. 7) between excitations of opposite pseudo-spins. For free fermions in the limit $T \rightarrow 0$, the asymptotic electron states of ISIM are stationary waves with even (odd) phase shifts $\delta_{e,o}(k)$ induced by the

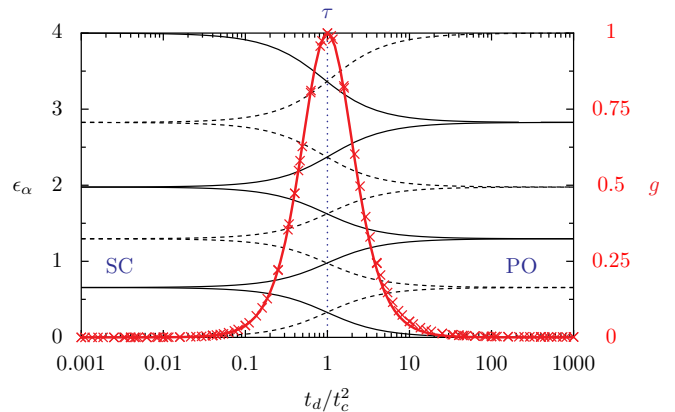


FIG. 8: (Color online) ϵ_α and g as a function of t_d/t_c^2 without interaction ($U = 0$). The values of g extracted from the NRG spectra (red cross) coincide with the exact values (Eq. (28) - red line).

scattering region

$$\Psi_e(k, p) \propto \cos(k(p - 1/2) - \delta_e(k)), \quad (23)$$

$$\Psi_o(k, p) \propto \sin(k(p - 1/2) - \delta_o(k)). \quad (24)$$

The shifts $\delta_{e,o}(k)$ of the scattering phases and $\delta\epsilon_{e,o}(k)$ of the energy levels are proportional for each pseudo-spin. This can be shown by taking a finite size L for ISIM, quantizing the momenta $k_{e,o}(n) = \pi n/L + \delta_{e,o}(k)/L$ and using the dispersion relation $\epsilon(k) = 2 \cos(k)$. This yields

$$\Delta\epsilon = (\delta\epsilon_e - \delta\epsilon_o) \propto (\delta k_e - \delta k_o) \propto (\delta_e - \delta_o). \quad (25)$$

In the limit $L \rightarrow \infty$, the quantum conductance $g(t_d)$ of ISIM can be expressed as a function of the scattering phase shifts:

$$g(t_d) = \sin^2(\delta_e(t_d) - \delta_o(t_d)). \quad (26)$$

From Eq. (25) and Eq. (26), one eventually obtains the relation which allows us to extract g from the NRG spectra:

$$g(t_d) = \sin^2\left(\pi \frac{\Delta\epsilon(t_d)}{\Delta\epsilon(t_d \rightarrow \infty)}\right). \quad (27)$$

The proportionality factor between $\Delta\epsilon(t_d)$ and $\delta_e(t_d) - \delta_o(t_d)$ has been determined from the condition that $g \rightarrow 0$ (for $\delta_e - \delta_o \rightarrow \pi$) when $t_d \rightarrow \infty$. Eq. (27) describes a quantum conductance which vanishes when $t_d \rightarrow 0$ and when $t_d \rightarrow \infty$, and reaches the unitary limit for an intermediate value $\tau(U, t_c)$ of t_d .

Let us check that the NRG algorithm and Eq. (27) give us the correct behavior for the conductance g in the non-interacting limit where it is straightforward to solve the scattering problem. One obtains

$$g(U = 0) = 4 \left(\frac{t_d}{t_c^2} + \frac{t_c^2}{t_d} \right)^{-2}. \quad (28)$$

The $\epsilon_\alpha(t_d)$ given by the NRG algorithm for $U = 0$ are shown in Fig. 8 with the corresponding values of g obtained from Eq. (27). One can see that the behavior of g given by the NRG algorithm and Eq. (27) reproduces the correct behavior given by Eq. (28) in the non-interacting limit.

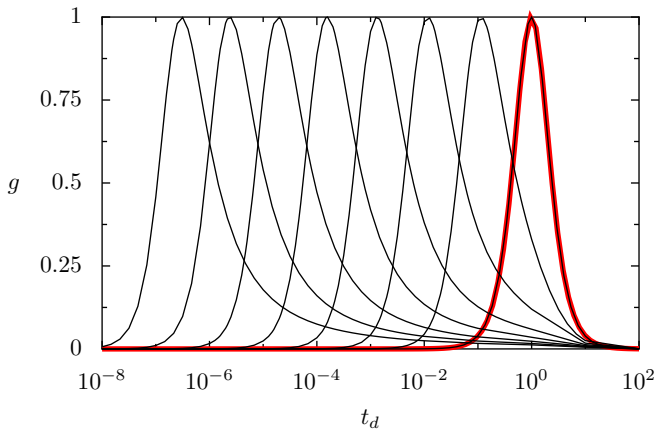


FIG. 9: (Color online) $g(t_d)$ extracted from the NRG spectra for $t_c = 1$ and many values of U . Increasing U shifts the transmission peaks to smaller values of t_d . The curves correspond respectively to $U = 0$ (red curve), 5, 10, 15, 20, 25, 30, 35.

X. UNIVERSAL PROPERTIES OF ISIM

In Fig. 9, the conductance g extracted from the NRG spectra using Eq. (27) is given as a function of t_d for a coupling term $t_c = 1$ and many values of U . The larger is U , the smaller is the characteristic scale $\tau(U)$. Fig. 9 seems to indicate that the left sides of the transmission peaks are simply translated to lower values of t_d as U increases. This is confirmed in Fig. 10a) where g is given as a function of the dimensionless scale t_d/τ , τ being obtained from the criterion $g(t_d = \tau) = 1$. The curves $g(t_d/\tau)$ obtained for $t_c = 1$ are shown in Fig. 10a), while the curves obtained for $t_c = 0.1$ and $t_c = 0.01$ have been added in Fig. 10(b). These figures show the main result of this study, i.e., When t_d is not too large, g is given by a universal function of $t_d/\tau(U, t_c)$. This function is independent of the values taken for U or t_c . Since $g(t_d)$ has been directly extracted from the free fermion NRG spectra, the NRG spectra must be also given by universal functions of $t_d/\tau(U, t_c)$, independent of the values of U and t_c . This is shown in Fig. 10(c) ($t_c = 1$) and in Fig. 10(d) ($t_c = 1, 0.1, 0.01$), where the first excitations ϵ_α obtained for NRG chains of large even length N are plotted as a function of t_d/τ .

The values of $\tau(U, t_c)$ used in Fig. 10 are given in Fig. 11. If one decreases the temperature T in the Anderson model without magnetic field, it has been shown in Ref. 10 that the interaction effects remain perturbative when $U < \pi\Gamma$ while they become non-perturbative when $U > \pi\Gamma$. Since the level width $\Gamma = t_c^2$ for the nanosystem used in ISIM at half-filling, we give the dimensionless scale τ/U as a function of U/t_c^2 in Fig. 11. One can see that τ/U has a slow decay followed by a faster decay, with a crossover around an interaction threshold consistent with the interaction threshold $\pi\Gamma$ characterizing the perturbative-non-perturbative crossover in the Anderson model. For ISIM, this suggests that the interaction effects upon g are perturbative when $U < \pi\Gamma$, and non-perturbative when $U > \pi\Gamma$. However, the universal behavior of $g(t_d/\tau)$

is not restricted to the non-perturbative ‘‘Kondo’’ regime, but characterizes also the perturbative regime.

A. Universality near the SC limit ($t_d \leq \tau$)

The universal regime can be divided into two parts. The first one begins at $t_d = 0$ in the vicinity of the SC fixed point and ends at $t_d = \tau$. In this SC regime, g behaves as without interaction, but with a renormalized level width ($t_c^2 \rightarrow \tau(U, t_c)$). As shown in Fig. 10, all the curves $g(t_d/\tau)$ are on a single universal curve when $t_d \leq \tau$, independent of the values of U and t_c . Since one of those curves (the red one) corresponds to the non-interacting limit $U = 0$, the universal curve for $t_d \leq \tau$ is given by Eq. (28) where t_d is measured in units of τ , instead of t_c^2 :

$$g(t_d, U, t_c) = 4 \left(\frac{t_d}{\tau(U, t_c)} + \frac{\tau(U, t_c)}{t_d} \right)^{-2}. \quad (29)$$

B. Universality around a LM limit ($\tau < t_d < t_c\sqrt{U}$)

The universal regime persists when t_d exceeds τ . While $g(t_d/\tau)$ decays immediately after the transmission peak if $U = 0$, $g(t_d/\tau)$ begins to follow a new part of the universal curve if $U \neq 0$. This new part is not given by Eq. (29), and ceases when a faster decay occurs. The larger is U , the larger is the interval of values of t_d/τ where $g(t_d/\tau)$ follows the slow decay of the universal curve (see Fig. 10). To describe this slow decay, one can use exact results which give the magnetization $m(h)$ of the Anderson model at $T = 0$ as a function of the magnetic field h . This will be done after a study of the relation between $g(t_d)$ and $m(h)$.

Let us just note now that the singlet state of the SC limit could be broken either if the temperature T or the ‘‘Zeeman energy’’ t_d exceeds the Kondo temperature T_K . This makes likely that the effects of T and t_d would be somewhat similar. If this is the case, the intermediate values of t_d would be related to the formation of a local moment in the equivalent Anderson model of ISIM, and an intermediate LM regime would take place between the SC regime for low values of t_d and the PO regime for large values of t_d . This classification is used in Ref. 14 for describing the effect of a magnetic field in the zero-temperature limit of the Anderson model. However, we can only refer to the SC, LM and PO regimes, and not to the SC, LM and PO fixed points. The RG flows of ISIM yielded by increasing t_d at $T = 0$ and by increasing T at $t_d = 0$ are very different. Increasing T in ISIM at $t_d = 0$ yields the 3 plateaus shown in Fig. 5, characteristic of 3 well-defined fixed points. There are no free fermions between the plateaus, since there are no $\epsilon_\alpha(T)$ such that $E_I(T) = \sum_\alpha \epsilon_\alpha(T)$ outside the plateaus. In contrast, Fig. 10 does not exhibit plateaus and the $E_I(t_d)$ can be described by a continuum of effective non-interacting spectra as t_d varies at $T = 0$, and not only by the three spectra of the SC, LM and FO fixed points.

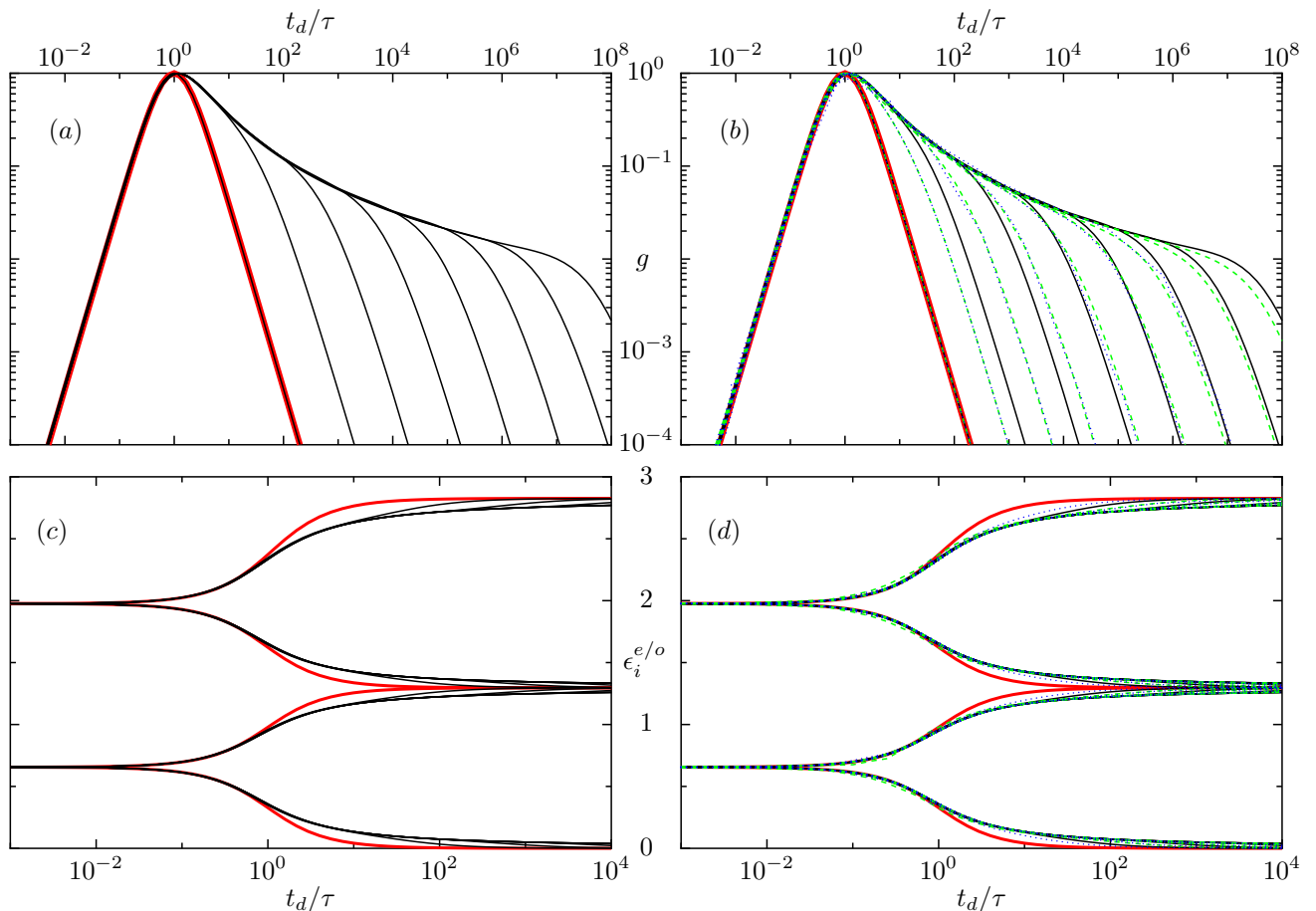


FIG. 10: (Color online) Figure 10(a): g as a function of t_d/τ for $t_c = 1$ and many values of U . τ has been determined from the criterion $g(t_d = \tau) = 1$. The larger is U , the larger are the values of t_d/τ where g decays. The curves correspond respectively to $U = 0$ (red curves) and $U = 5, 10, 15, 20, 25, 30, 35$ (black curves). Figure 10(b): g as a function of t_d/τ . To the data (black curves) calculated taking $t_c = 1$ and shown in Fig. 10(a), we have added the data calculated taking $t_c = 0.1$ and $U = 0$ (red curve), 0.05, 0.1, 0.15, 0.2, 0.25, 0.3, 0.35, 0.4 (green dashed curves) and taking $t_c = 0.01$ and $U = 0$ (red curve), 0.0005, 0.001, 0.0015, 0.002, 0.0025, 0.003, 0.0035 (blue dotted curves). Figure 10(c): First one body excitations ϵ_α for N even as a function of t_d/τ . Same values of t_c and U as in Fig. 10(a). Figure 10(d): ϵ_α for N even as a function of t_d/τ . Same values of t_c and U as in Fig. 10(b).

C. Interaction-independent conductance in the PO limit ($t_d > t_c\sqrt{U}$)

As one increases t_d/τ , $g(t_d/\tau)$ eventually exhibits a fast decay which is not given by a universal function of t_d/τ . As can be seen in Fig. 10, this fast decay corresponds to the decay of $g(t_d/t_c^2)$ obtained without interaction, but shifted to values of t_d/τ which increase when U increases. According to Ref. 14, the Anderson model at $T = 0$ is in a LM regime if the magnetic field h lies in the interval $T_K < h < h^* \propto \sqrt{UT}$. The upper threshold \sqrt{UT} appears in the Hartree-Fock study made by Anderson²⁴ of the transition from the non-magnetic to the LM regime of the Anderson model, as one decreases T without magnetic field. For ISIM, this suggests that the slow universal decay of $g(t_d/\tau)$ corresponding to the LM regime persists as far as $t_d < t_d^* \propto t_c\sqrt{U}$. Above t_d^* , ISIM should enter in the PO regime. This is confirmed in Fig. 12, where one can see that g becomes independent of U and be-

haves as without interaction when t_d exceeds a threshold value $t_d^* \approx 10\sqrt{UT}$.

XI. CHARACTERISTIC ENERGY SCALE IN THE PERTURBATIVE REGIME

Without interaction, Eq. (28) implies that $g = 1$ if $t_d = t_c^2$. This yields for the characteristic energy scale τ of ISIM a non-interacting value t_c^2 . For weak values of U , there is a perturbative regime where g and τ can be obtained using self-consistent Hartree-Fock theory. In the symmetric case, the Hartree corrections and the site potentials V_G cancel each others since $V_G = -U/2$. The value of the inter-site hopping t_d is modified because of exchange and takes⁵ a value given by the self-consistent solution of the HF equation

$$v = t_d + U \langle c_0^\dagger c_1(v, t_c) \rangle. \quad (30)$$

Using Eq. (28) with v instead of t_d gives the HF value of g .

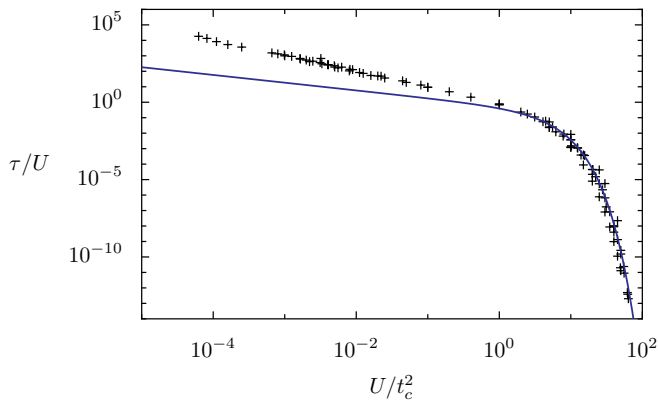


FIG. 11: (Color online) Characteristic scale $\tau(U, t_c)$ as a function of U and t_c . The values of $\tau(U, t_c)/U$ obtained from the condition $g(t_d/\tau) = 1$ and used in Fig. 10 are plotted as a function of $x = U/t_c^2$ (+). The solid blue line $y(x) = 0.728\sqrt{2}/(\pi x) \exp(-\pi x/8)$ fits the data in the non-perturbative regime and corresponds to the relation $\tau = 2T_K$ with $T_K = 0.364\sqrt{2t_c^2 U/\pi} \exp(-\pi U/8t_c^2)$.

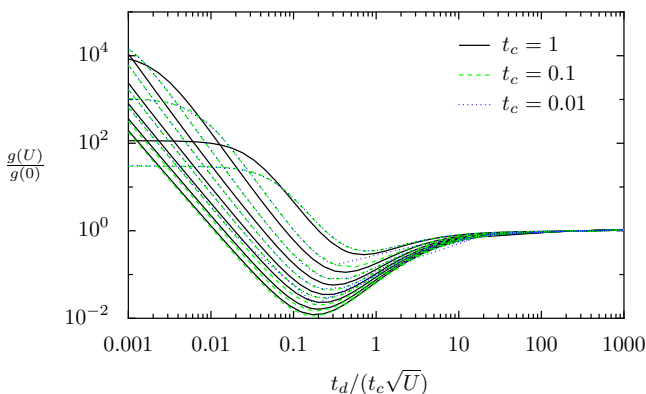


FIG. 12: (Color online) Ratio $g(U, t_c, t_d)/g(U = 0, t_c, t_d)$ as a function of $t_d/(t_c\sqrt{U})$. $g(U)$ is extracted from the NRG spectrum and $g(U = 0)$ is given by Eq. (28). One can see that g behaves as without interaction when $t_d > t_d^* \approx 10t_c\sqrt{U}$. Same values of t_c and U as in Fig. 10.

For the Anderson model, it is well known that HF theory fails to describe the Kondo regime. This Kondo regime occurs when the interaction exceeds a threshold value $\pi\Gamma$, either for low temperatures $T < T_K$ without magnetic field h , or for weak fields $h < T_K$ at $T = 0$. In the frame of the HF approximation, a magnetic moment should be formed, while it actually vanishes because of strong correlations between the conduction electrons and the impurity spin (Kondo effect). Therefore, one does not expect that HF theory should be valid in the orbital Kondo regime of ISIM for large values of U ($U > \pi\Gamma$) and small values of t_d if $T = 0$.

For a large coupling $t_c = 1$, the results shown in Fig. 13 confirm this prediction: HF theory gives the correct value of g for all values of t_d as far as U remains smaller than πt_c^2 . For $U > \pi t_c^2$, the HF curves and the NRG curves coincide only when t_d is large ($t_d > \tau$), but become very different at the left side of the transmission peak. For a small coupling

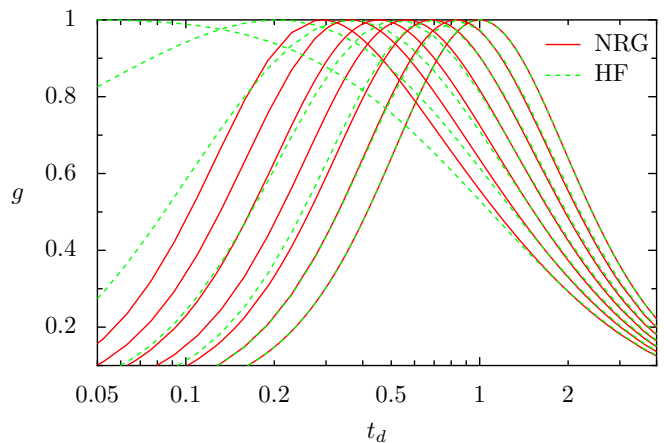


FIG. 13: (Color online) Conductance g as a function of t_d for $t_c = 1$ and $U = 0, 0.5, 1, 1.5, 2, 2.5, 3$. g extracted from the NRG spectra (solid red curves) coincides with the HF estimates (dashed green curves) when $U < t_c^2$ or for $t_d \gg t_c\sqrt{U}$ if $U > t_c^2$.

$t_c = 0.1$, one can see in Fig. 14 a more dramatic breakdown of HF theory which fails to give the peak of perfect transmission (see the curves with $U = 0.04$ and more notably $U = 0.05$ of Fig. 14).

The origin of this failure can be simply explained. In the perturbative regime where g is given by Eq. (28) with v instead of t_d , $g = 1$ if $v = t_c^2$. This yields for the scale τ a HF value

$$\tau_{HF} = t_c^2 - A(t_c)U, \quad (31)$$

where the function

$$A(t_c) = \langle c_0^\dagger c_1(v = t_c^2, t_c) \rangle, \quad (32)$$

which is shown in Fig. 15, depends weakly on t_c ($A = 1/\pi$ if $t_c = 1$ while $A \rightarrow 1/4$ if $t_c \rightarrow 0$). When U reaches a value t_c^2/A , HF theory predicts that the interaction should renormalize t_d to a value $\tau_{HF} = 0$ for having $g = 1$! This is absurd and confirms that HF theory breaks down for ISIM above an interaction threshold which is essentially the same as for the Anderson model ($U > \pi\Gamma$).

In the non-perturbative regime of the Anderson model, the physical quantities such as the magnetization m must be universal functions of T/T_K or h/T_K . This means that τ should be related to the characteristic temperature T_K of the orbital Kondo effect yielded by the inversion symmetry of ISIM. The relation between τ and T_K can be obtained using Friedel sum rule and analytical results for the magnetization $m(h)$ of the Anderson model at zero temperature.

XII. IMPURITY OCCUPATION NUMBERS AND SCATTERING PHASE SHIFTS

For having g , another method consists in using NRG for calculating the average impurity occupation numbers $\langle n_{e/o} \rangle$ of the even and odd orbitals of the nanosystem. The difference

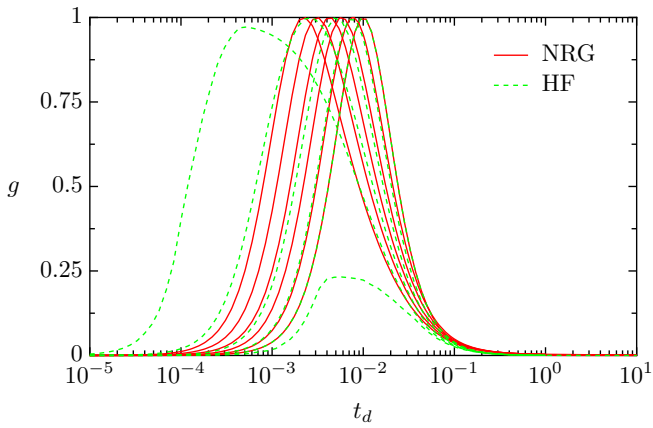


FIG. 14: (Color online) Conductance g as a function of t_d for $t_c = 0.1$ and $U = 0, 0.01, 0.02, 0.03, 0.04$ and $U = 0.05$. The NRG results (solid red curves) and the HF results (dashed green curves) coincide for $U < t_c^2$. For $U = 0.05$, the HF curve gives only a small peak where $g \approx 0.25$, and not $g = 1$.

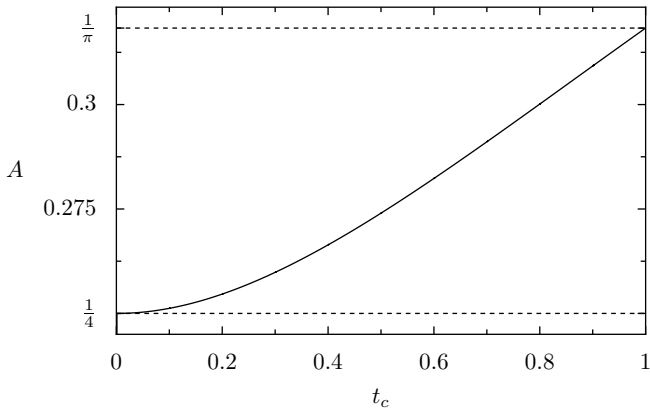


FIG. 15: Function $A(t_c)$ defined in Eq. (32) as a function of t_c .

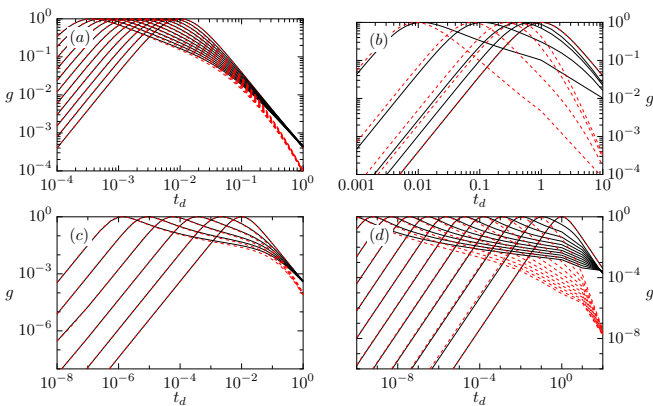


FIG. 16: (Color online) Values of g obtained from the NRG spectrum (black solid lines, Eq. (27)) and approximate values \tilde{g} (red dashed lines, Eq. (33)), as a function of t_d . Increasing U moves the conductance peak towards the left side. Figure (a): $t_c = 0.1$ and $U = 0, 0.01, 0.02, \dots, 1$. Figure (b): $t_c = 1$ and $U = 0, 1, 2, 5, 10$. Figure (c): $t_c = 0.1$ and $U = 0, 0.05, 0.1, 0.15, 0.2, 0.25$. Figure (d): $t_c = 1$ and $U = 0, 5, 10, 15, \dots, 55$.

between the scattering phase shifts can be given in terms of $\langle n_{e/o} \rangle$, if one assumes an approximate form of the Friedel sum rule (FSR):

$$\delta_e - \delta_o \approx \pi (\langle n_e \rangle - \langle n_o \rangle), \quad (33)$$

and one gets an approximate value \tilde{g} for g from this estimate of $\delta_e - \delta_o$ using Eq. (26):

$$\tilde{g} = \sin^2(\pi (\langle n_e \rangle - \langle n_o \rangle)). \quad (34)$$

This approximate FSR is often used (see for instance Ref. 30) and allows us to obtain g from the zero temperature impurity magnetization $m(h)$ of the Anderson model with magnetic field h . This is particularly interesting since $m(h)$ is a physical quantity for which exact results have been obtained with the Bethe-Ansatz by Tsvetick and Wiegmann. Unfortunately, Eq (33) is only an approximation, and not the true FSR, as pointed out by Simon and Affleck in a study³¹ of persistent currents through a quantum dot at Kondo resonance. The generalization of FSR by Langreth^{13,32} shows that the phase shifts are proportional to the number of electrons displaced by the impurity, “among which are included not only the d electrons, but also some of the conduction electrons”. For ISIM, this means that the displaced electrons are not only those inside the interacting region, but displaced electrons in the neighboring parts of the leads have to be included too for obtaining the phase shifts from the occupation numbers via FSR. At first sight, one can expect that Eq. (33) could be used only if the scattering region is weakly coupled to the attached leads. Our results show that this is less simple.

The difference between the values of g obtained directly from the NRG spectra [Eq. (27)] and the approximated values \tilde{g} are given as a function of t_d for weak ($t_c = 0.1$, Fig. 16a and d) and large values ($t_c = 1$, Fig. 16b and c) of the coupling, and for weak (Fig. 16a and c) or large values (Fig. 16b and d) of U . Even for a weak coupling $t_c = 0.1$, where one could expect a negligible displaced charge outside the nanosystem, $\tilde{g} = g$ only when ISIM is near the SC fixed point ($t_d \leq \tau$). When $t_d > \tau$, $\tilde{g} \neq g$. For a larger coupling ($t_c = 1$), one can notice also differences between g and \tilde{g} even when $t_d \leq \tau$ in the perturbative regime ($U < \pi t_c^2$). One concludes that g can be obtained from \tilde{g} with a good accuracy only in the non-perturbative regime where ISIM exhibits an orbital Kondo effect ($U > t_c^2/A$ and $t_d \leq \tau$). Otherwise, the difference $\delta_e - \delta_o$ is not given by the difference $\langle n_e \rangle - \langle n_o \rangle$ evaluated inside the nanosystem, but depends also on the occupation numbers outside the nanosystem.

The validity of the approximate FSR in the non-perturbative regime when $t_d < \tau$ can be explained by the following argument: the conduction electrons which are displaced to screen the impurity pseudo-spin (forming a singlet state with the impurity) are only a negligible fraction $\approx T_K/E_F$ of the conduction electrons. To neglect this fraction induces an error $\propto \tau/t_h$ which cannot be seen in the curves shown in Fig. 16 when τ is very small (see Fig. 11). When the system is not in the orbital Kondo regime ($U < \pi t_c^2$ or $t_d > \tau$), the number of displaced electrons becomes much larger, and the difference between g and \tilde{g} can be seen in Fig. 16.

XIII. ZERO TEMPERATURE MAGNETIZATION OF THE SYMMETRIC ANDERSON MODEL

The exact solution of the Anderson model can be obtained using Bethe-Ansatz. Tsvetick and Wiegmann have solved the Bethe-Ansatz equations for the Anderson model in an arbitrary magnetic field. Let us summarize their results^{14,15} for the symmetric case, which were obtained assuming the continuum limit and an infinite bandwidth ($t_h \rightarrow \infty$) for an Anderson impurity coupled to a 3D bath of non-interacting electrons. Since the bath for ISIM is provided by non-interacting electrons free to move on a semi-infinite 1D tight-binding lattice, and since we give results for values of t_c , t_d and U which are not always small compared to t_h , one cannot rule out certain quantitative differences between the results of Refs. 14, 15 and our numerical results. This may concern the numerical prefactors in the expression of T_K or the constants in the universal functions describing the magnetization $m(h)$. However, a qualitative agreement should be expected. The Kondo temperature of the Anderson model reads

$$T_K = F \sqrt{U t_c^2} \exp - \left(\frac{\pi U}{8 t_c^2} \right), \quad (35)$$

where F is a prefactor which depends on the definition of T_K (which varies¹⁴ from one author to another) and is modified³³ if the bandwidth of the bath of conduction electrons is finite or infinite. $F = \sqrt{2}/\pi$ for the infinite bandwidth Anderson model^{14,15}, while $F = 0.364\sqrt{2}/\pi$ if the bandwidth is taken finite³³.

When $U \geq \Gamma$ (non-perturbative regime), the Bethe-Ansatz results for the impurity magnetization $m(h)$ can be divided in three characteristic regimes as the magnetic field h increases at $T = 0$.

A SC regime for low fields ($h < T_K$) where the magnetization is given by a universal function of h/T_K :

$$m(h) = \frac{h}{2\pi T_K}, \quad (36)$$

followed by a LM regime for intermediate fields ($T_k < h < \sqrt{U\Gamma}$) where $m(h)$ is given by another universal function of h/T_K which can be expanded as

$$m(h) \approx \frac{1}{2} \left(1 - \frac{1}{\ln(\frac{h}{T_K})} + \dots \right), \quad (37)$$

before having a PO regime for strong fields ($h > \sqrt{U\Gamma}$) (denoted FO regime in Ref. 14) where

$$m(h) \approx \frac{1}{2} \left(1 - \frac{2\Gamma}{\pi h} + \dots \right) \quad (38)$$

becomes independent of the interaction U .

When $U \approx \Gamma$, there is direct transition from a non-magnetic regime where $m(h) \approx h/\Gamma$ towards the free orbital regime where the behavior of $m(h)$ is given by Eq. (38).

XIV. CHARACTERISTIC ENERGY SCALE AND UNIVERSAL SCALING FUNCTIONS

In the perturbative regime ($U < \pi t_c^2$), the conductance is well described by HF theory, which yields $g = 4/(v/t_c^2 + t_c^2/v)^2$ with v given by Eq. (30). The scale τ takes a value τ_{HF} given by Eq. (31).

In the non-perturbative regime ($U > \pi t_c^2$), let us revisit our numerical results for g using the exact expressions giving the magnetization $m(h)$ for an Anderson model (3D bath of conduction electrons, wide band limit where $t_h \rightarrow \infty$) which is not exactly the Anderson model corresponding to ISIM.

The conductance $\tilde{g}(t_d)$ reads

$$\tilde{g}(t_d) = \sin^2(2\pi m(t_d)) \quad (39)$$

where $m(t_d)$ is the pseudo-magnetization of the nanosystem with pseudo-spin 1/2 and reads

$$m(t_d) = \frac{\langle n_e(t_d) \rangle - \langle n_o(t_d) \rangle}{2}. \quad (40)$$

In the SC limit ($t_d < T_K$) where g and \tilde{g} coincide, this gives

$$\tilde{g}(t_d) = \sin^2(t_d/T_k) \approx \left(\frac{t_d}{T_k} \right)^2 \approx g(t_d), \quad (41)$$

while the conductance g extracted from the NRG spectra reads

$$g(t_d) = \left(\frac{2}{t_d/\tau + \tau/t_d} \right)^2 \approx 4 \left(\frac{t_d}{\tau} \right)^2. \quad (42)$$

This yields a relation between the characteristic scale τ of ISIM and the Kondo temperature T_K of the Anderson model:

$$\tau(U, t_c^2) = 2T_K(U, t_c^2). \quad (43)$$

Using for T_K Eq. (35) with the finite bandwidth prefactor $F = 0.364\sqrt{2}/\pi$ given in Ref. 33, one gets for τ the analytical expression

$$\tau(U, t_c) = 0.728 \sqrt{\frac{2t_c^2 U}{\pi}} \exp - \left(\frac{\pi U}{8t_c^2} \right). \quad (44)$$

Eq. (44) describes very well the numerical values of $\tau(U, t_c)$ obtained from the NRG spectra and the condition $g(t_d = \tau) = 1$ in the non-perturbative regime, as shown in Fig. 11 for $U > t_c^2/A$. Moreover, the behavior of g calculated for $U = 0.25$ and $t_c = 0.1$ is given in Fig. 17 as a function of t_d when $t_d < \tau$. One can see that the expression $\tilde{g} = \sin^2(2t_d/\tau)$ with the value of τ calculated from Eq. (44) ($\tau = 1.582510^{-6}$) describes the behavior of g or \tilde{g} calculated using the NRG algorithm when $t_d < \tau$.

Fig. 18 gives the NRG values of g and \tilde{g} as a function of t_d for $U = 0.25$ and $t_c = 0.1$ in the LM regime. One can see that $g \approx \tilde{g}$ around the transmission peak, but becomes slightly different when $t_d > \tau$. Using Eq. (37) for $m(t_d)$, the NRG values of $\tilde{g}(t_d)$ shown in Fig. 18 are not reproduced by $\sin^2(2\pi m(t_d))$. We explain this failure by the fact that the Anderson model corresponding to Eq. (37) is not exactly

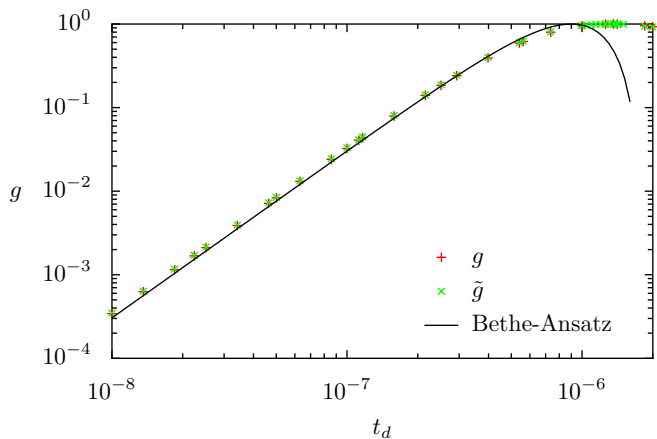


FIG. 17: (Color online) SC regime: Values of g (red plus), \tilde{g} (green cross) obtained from the NRG algorithm and Bethe-Ansatz expression $\sin^2(2t_d/\tau)$ (solid line) as a function of t_d for $U = 0.25$ and $t_c = 0.1$. The value of τ used in the Bethe-Ansatz expression have been obtained from the relation $\tau = 2T_K$, with T_K given by Eq. (44).

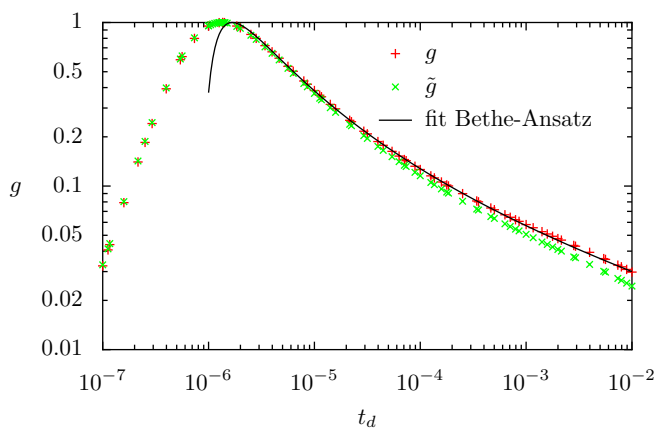


FIG. 18: (Color online) LM regime: NRG values of g (red plus) and \tilde{g} (green cross) as a function of t_d for $U = 0.25$ and $t_c = 0.1$. The solid line (fit Bethe-Ansatz) corresponds to Eq. (45) with the value of $\tau = 2T_K$ given by Eq. (44) and used in Fig. 17.

the Anderson model corresponding to ISIM. This might give different constants in the function given in Eq. (37). However, we have been able to find a function of $X = t_d/\tau$ inspired by the form of $m(h/T_K)$ given in Eq. (37) and which fits very well the values of g in the LM regime:

$$g(X) = \sin^2 \left(\pi \left(2.0175 - \frac{0.7388}{\ln(2.8573X)} \right) \right). \quad (45)$$

As shown in Fig. 18, such a fit with the value of $\tau = 2T_K$ used in Fig. 17 allows us to describe $g(t_d)$. Eq. (45) gives an excellent approximation of the universal curve of $g(t_d/\tau)$ in the LM regime.

When $t_d > t_c\sqrt{U}$ (PO regime), g can be described by the non-interacting expression $4(t_d/t_c^2 + t_c^2/t_d)^{-2}$, which achieves the complete description of $g(t_d, U, t_c)$ in the symmetric case by analytical expressions.

XV. SUMMARY AND PERSPECTIVE

When $t_d \leq \tau$, we have shown that the quantum conductance is given by a universal function of the ratio $X = t_d/\tau$ of two energies. This universal function $g(X) = 4(X + X^{-1})^{-2}$ characterizes the non-interacting limit, where the isolated nanosystem has two levels of energy $V_G \pm t_d$ with a level spacing $\Delta = 2t_d$. Those levels have a width $\Gamma = t_c^2$ when the nanosystem is coupled to leads at $E_F = 0$. Therefore the ratio X is also the ratio $\Delta/2\Gamma$. We have found that $g(X)$ remains unchanged when the electrons interact inside the nanosystem, if one adds a term $\propto U$ to the broadening Γ in the perturbative regime. When U becomes larger, there is a non-perturbative regime where a more complicated many-body resonance appears at E_F . In that case, the relation $\tau = 2T_K$ which we have obtained is consistent with the fact that the width Γ of the nanosystem levels becomes the Kondo temperature T_K . We have thus shown that the interaction U leaves the function $g(X)$ unchanged in the SC regime, renormalizing only the level broadening Γ .

To have a conductance which is given by the ratio of two characteristic energies and which stays at zero temperature on a universal curve when this ratio varies is reminiscent of the scaling theory of localization³⁴. Recently, it has been found³⁵ using numerical Quantum Monte Carlo simulations that the $\beta(g)$ -function characterizes not only the non-interacting limit³⁴, but also 2D disordered systems with Coulomb interactions. We have given another example of a universal function which remains unchanged when the electrons interact, the interaction renormalizing only the characteristic scale (Γ for the dimensionless ratio Δ/Γ in this study, the localization length ξ for the dimensionless ratio L/ξ in 2D disordered systems³⁵).

When $\tau < t_d < t_c\sqrt{U}$, a local moment is formed in the equivalent Anderson model and the universal function $g(X)$ is not given by the non-interacting limit. Adapting an analytical expression describing the magnetization of the Anderson model, we have proposed an analytical form which reproduces the universal function $g(X)$ in the LM regime.

We have shown that the interacting region becomes perfectly transparent when $t_d = \tau$. In the non-perturbative regime, this corresponds to a nanosystem level spacing $\Delta \approx T_K$. This result shown using ISIM is a particular illustration of the minimal realization of the orbital Kondo effect in a quantum dot with two leads, which has been studied by Silvestrov and Imry³⁶ for more general setups. The role of the conduction electron spin is played by the lead index in Ref. 36, while it is played by the even and odd orbitals for ISIM. In the two cases, the Kondo effect takes place if there are two close levels in a dot populated by a single electron, and the conductance at $T = 0$ is zero at the SU(2) symmetric point ($t_d = 0$ for ISIM), while it reaches the unitary limit $G = e^2/h$ for some finite value $\approx T_K$ of the level splitting Δ . However, the prediction made in Ref. 36, that for temperature $T > T_K$ the conductance becomes maximal if the levels are exactly degenerate, cannot be valid for ISIM where level degeneracy means no coupling between the left and right leads ($t_d = 0$).

We have shown that the quantum conductance of an inter-

acting nanosystem coupled to non-interacting 1D leads can be described with a universal function $g(X)$. This concept, with a similar function $g(X)$, must remain valid if one couples the nanosystem to non-interacting 2D or 3D leads instead of strictly 1D leads. This can be understood if one considers the Anderson models of pseudo-spin 1/2 particles corresponding to ISIM with leads of dimension D . The Kondo physics of such models, where the quantum impurity is coupled to a bath of dimension D , is qualitatively independent of the used bath. A change of the dimension of the leads modifies only the dependence of the nanosystem level width Γ upon t_c ($\Gamma \propto t_c^2$ in all dimensions D , but with factors which depend on D), and hence the dependence of the Kondo temperature upon t_c . This makes likely that the universal aspects of g obtained in a pure 1D limit using ISIM do characterize also more general spinless models, where the nanosystem and the leads would be created in gated 2D semiconductor heterostructures. In that case, ISIM is a simplified model which could describe quantum transport of spin polarized electrons through an inversion-symmetric double-dot setup, as a function of the inter-dot coupling. Since such a coupling can be

easily varied if the two dots are coupled by a quantum point contact, it will be interesting to check whether the quantum conductance of such setup is given by a universal function of the dimensionless inter-dot coupling t_d/T_K when $T \rightarrow 0$. For observing the orbital Kondo regime using such a setup, a large capacitive inter-dot coupling will be necessary. It will be also interesting to introduce the spin 1/2 of electrons in ISIM for studying the role of t_d upon the SU(4)-Kondo effect, as we have studied its role upon the SU(2)-Kondo effect using spinless fermions. The possibility of observing SU(4)-symmetric Fermi liquid state in a symmetric double quantum dot system with strong capacitive inter-dot coupling has been discussed in Ref. 27.

Eventually, this study was restricted to the symmetric case, leaving to a following work the study of the asymmetric case ($E_F \neq 0$, $V_G \neq -U/2$), where the role of t_d upon the valence-fluctuation fixed point remains to be investigated.

We thank Denis Ullmo for very useful discussions and the RTRA “Triangle de la Physique” of Palaiseau-Orsay-Saclay for financial support.

-
- ¹ Y. Meir and N. S. Wingreen, Phys. Rev. Lett. **68**, 2512 (1992).
² R. A. Molina, P. Schmitteckert, D. Weinmann, R. A. Jalabert, G.-L. Ingold, and J.-L. Pichard, Eur. Phys. J. B **39**, 107 (2004).
³ R. A. Molina, D. Weinmann, and J.-L. Pichard, Eur. Phys. J. B **48**, 243 (2005).
⁴ D. Weinmann, R. A. Jalabert, A. Freyn, G.-L. Ingold, and J.-L. Pichard, Eur. Phys. J. B **66**, 239 (2008).
⁵ Y. Asada, A. Freyn, and J.-L. Pichard, Eur. Phys. J. B **53**, 109 (2006).
⁶ A. Freyn and J.-L. Pichard, Phys. Rev. Lett. **98**, 186401 (2007).
⁷ A. Freyn and J.-L. Pichard, Eur. Phys. J. B **58**, 279 (2007).
⁸ A. Freyn, I. Kleftogiannis and J.-L. Pichard, Phys. Rev. Lett. **100**, 226802 (2008).
⁹ H. R. Krishna-murthy, K. G. Wilson, and J. W. Wilkins, Phys. Rev. Lett. **35**, 1101 (1975).
¹⁰ H. R. Krishna-murthy, J. W. Wilkins, and K. G. Wilson, Phys. Rev. B **21**, 1003 (1980).
¹¹ H. R. Krishna-murthy, J. W. Wilkins, and K. G. Wilson, Phys. Rev. B **21**, 1044 (1980).
¹² R. Bulla, T. A. Costi, and T. Pruschke, Rev. Mod. Phys. **80**, 395 (2008).
¹³ A. C. Hewson, *The Kondo Problem To Heavy Fermions* (Cambridge University Press, 1993).
¹⁴ A. M. Tsvelick and P. B. Wiegmann, Advances in Phys. **32**, 453 (1983).
¹⁵ P. B. Wiegmann and A. M. Tsvelick, J. Phys. C: Solid State Phys. **16**, 2281 (1983).
¹⁶ D. Goldhaber-Gordon, H. Shtrikman, D. Mahalu, D. Abusch-Magder, U. Meirav, and M. A. Kastner, Nature (London) **391**, 156 (1998).
¹⁷ S. M. Cronenwett, T. H. Oosterkamp, and L. P. Kouvanhoven, Science **281**, 540 (1998).
¹⁸ M. Grobis, I. G. Rau, R. M. Potok, H. Shtrikman, and D. Goldhaber-Gordon, Phys. Rev. Lett. **100**, 246601 (2008).
¹⁹ T. Delattre, C. Feuillet-Palma, L. G. Herrmann, P. Morfin, J.-M. Berroir, G. Fève, B. Placais, D. C. Glattli, M.-S. Choi, C. Mora, and T. Kontos, Nature Physics **5**, 208 (2009).
²⁰ R. K. Kaul, G. Zaránd, S. Chandrasekharan, D. Ullmo, and H. U. Baranger, Phys. Rev. Lett. **96**, 176802 (2006).
²¹ P. Mehta and N. Andrei, Phys. Rev. Lett. **96**, 216802 (2006).
²² E. Boulat, H. Saleur, and P. Schmitteckert, Phys. Rev. Lett. **101**, 140601 (2008).
²³ A. Dhar, D. Sen, and D. Roy, Phys. Rev. Lett. **101**, 066805 (2008).
²⁴ P. W. Anderson, Phys. Rev. B **124**, 41 (1961).
²⁵ A. C. Hewson, Phys. Rev. Lett. **70**, 4007 (1993).
²⁶ A. C. Hewson, J. Bauer, and W. Koller, Phys. Rev. B **73**, 045117 (2006).
²⁷ L. Borda, G. Zaránd, W. Hofstetter, B. I. Halperin, and J. von Delft, Phys. Rev. Lett. **90**, 026602 (2003).
²⁸ W. Hofstetter and G. Zarand, Phys. Rev. B **69**, 235301 (2004).
²⁹ A. Oguri and A. C. Hewson, J. Phys. Soc. Jpn. **74**, 988 (2005).
³⁰ T. K. Ng and P. A. Lee, Phys. Rev. Lett. **61**, 1768 (1988).
³¹ P. Simon and I. Affleck, Phys. Rev. **64**, 085308 (2001).
³² D. C. Langreth, Phys. Rev. **150**, 516 (1966).
³³ F. D. M. Haldane, J. Phys. C: Solid State Phys. **11**, 5015 (1978).
³⁴ E. Abrahams, P. W. Anderson, D. C. Licciardello, and T. V. Ramakrishnan, Phys. Rev. Lett. **42**, 673 (1979).
³⁵ G. Fleury and X. Waintal, Phys. Rev. Lett. **100**, 076602 (2008).
³⁶ P. G. Silvestrov and Y. Imry, Phys. Rev. B **75**, 115335 (2007).